

Characterizing falling snow using multi-frequency dual-polarization measurements

Jani Tyynelä and V. Chandrasekar

Department of Electrical and Computer Engineering, Colorado State University, Fort Collins, CO 80523

36th Conference on Radar Meteorology, Breckenridge, Colorado, September 2013

1. INTRODUCTION

Radar reflectivities can be used to estimate rainfall/snowfall rates, dual-frequency ratios of radar reflectivities can be used to identify hydrometeor types, while polarimetric radar measurements can be used to estimate rainfall/snowfall rates, cloud ice-water content, identify hydrometeor types, and detect hail. Studies that combine polarimetric measurements at different frequencies in order to better characterize snow are less common.

Ground-based weather radars usually operate at lower microwave frequencies (S, C and X bands), where the return signal is not sensitive to the exact shape of snowflakes. On the other hand, higher frequencies are becoming more common in space-based radars and radiometers on satellites, such as NASA's Tropical Rainfall Measurement Mission (Ku), Global Precipitation Measurement Mission (Ku and Ka), CloudSat (W), and ESA's EarthCARE (W), on aircrafts, such as the NASA APR2 radar (Ku and Ka), and on mobile ground-based radars, such as the NASA D3R radar (Ku and Ka). Many of these instruments are used at polar latitudes, where most of the precipitation that reaches the ground is frozen and can accumulate as snowpacks during the winter season. It is therefore necessary to monitor the effect of snow on the environment both in local and global scale. The availability of simultaneous multi-frequency dual-polarization radar measurements can help to constrain the inverse problem of characterizing falling snow from the measurements.

Past studies have shown the importance in capturing the irregular structure and shape of falling snowflakes when their size reach wavelength scale (Westbrook et al. 2006; Ishimoto 2008; Petty and Huang 2010; Tyynelä 2011). As even single ice crystals exhibit a large morphological variation, as shown by the classification systems, adding precipitation processes, such as aggregation, riming, melting and breakup along the vertical column, further complicates the snow characterization from remote sensing observations. To help solve this inverse problem, it is therefore crucial to make in situ measurements of the physical properties of

the falling snow in order to constrain the unknown factors. The most important physical properties for snow are particle size, number density and mass as a function of size, and aspect ratio. These are all strongly affected by the ice crystal habit.

In this manuscript, we model pristine ice crystals of various types and their aggregates, use the discrete-dipole approximation (DDA) to compute backscattering properties from the modeled snow particles, and compare the backscattering properties to radar observations obtained in the GPM Cold-season Precipitation Experiment (GCPEX) during the winter of 2012. We present a case study that demonstrates how the forward modeling can be applied to multi-frequency dual-polarization measurements in order to characterize falling snow. We also analyze the backscattering properties using cluster validation indices (CVIs), which are statistical properties of a data set that measure how clustered it is with respect to the backscattering properties. This analysis helps us to choose, which measurements and their combinations provide best characterization.

2. NUMERICAL METHODS

Due to the importance of shape in scattering at the resonance regime (size parameter $x=ka>1$, where k is the wavenumber of the incident wave and a the volume-equivalent-sphere radius of the particle), it is crucial to use a physically realistic model for the various shapes for snowflakes and ice crystals. In the present study, we use six different pristine ice crystal types: hexagonal column, hexagonal plate, needle, ordinary dendrite, fern-like dendrite, and six-bullet rosette, covering most of the common types occurring at various atmospheric conditions and altitudes. In order to mimic natural shapes, we use the measured thickness-to-diameter and length-to-diameter ratios reported by Pruppacher and Klett (1997) for the different types of ice crystals.

For the purpose of comparison, we also include lump graupel generated with the fractal model by Ishimoto (2008). For generating graupel, the fractal

* Corresponding author address: Jani Tyynelä, Colorado State University / Department of Electrical and Computer Engineering, Fort Collins, CO 80523; e-mail janityynela@gmail.com.

Snowflake type	Size range [mm]	D0 [mm]
hexagonal column (N1e)	0.1-2.0	0.3-0.8
hexagonal plate (P1a)	0.1-2.0	0.3-0.8
needle (N1a)	0.5-3.0	0.7-1.3
ordinary dendrite (P1e)	0.5-5.0	0.8-1.8
fern-like dendrite (P1f)	1.0-8.0	1.6-3.0
six-bullet rosette (C3b)	0.1-0.6	0.3-0.6
lump graupel (R4b)	0.5-5.0	0.6-1.2
aggr. of needles	0.5-8.0	0.9-3.4
aggr. of ordinary dendrites	0.5-17.8	1.4-5.6
aggr. of fern-like dendrites	1.0-24.0	2.4-9.4
aggr. of rosettes	0.1-4.4	0.8-1.5

Table 1: Snowflake size distributions for the shape models.

dimension of 2.7 was chosen in order to get a decent fit to the measured mass -diameter relationship.

To generate realistic aggregates, we use the physically-based aggregation model by Westbrook (2004). We use four types of aggregate snow: aggregates of needles, ordinary dendrites, fernlike dendrites, and six-bullet rosettes. The number of crystals in each aggregate is varied and depends on the ice crystal type. For needles and dendrites, we use 2, 10, 20, 30, 40, and 50 monomers, while for the six-bullet rosettes, we use 2, 5, 10, 15, and 20.

Single ice crystals tend to fall in preferential orientation (e.g., Cho et al. 1981; Noel and Sassen 2005). To simulate this, we orient the generated ice crystals according to the measurements by Noel (2005) for warmer clouds, which indicate highly horizontal orientation with an average canting angle of about 2 deg and a Gaussian distribution with a standard deviation of 1 deg. It should be noted that these values are based on observations of planar crystals and may not be representative of all the types used in this study. The orientation of the aggregates is assumed to be random, although a recent study by Hogan (2012) indicates a preferential orientation. The average aspect ratio for all the modeled aggregate types is close to 0.6.

Examples of the modeled shapes for the different ice crystal types and their aggregates are shown in Fig. 1. Note that we only model dry pristine particles and their aggregates.

In Fig. 2, we show the mass of both the modeled single ice crystals and the measured values from various field studies as a function of the maximum horizontal diameter. The agreement between the measurements and the shape models is overall good, but some crystal types, such as the single dendrites exhibit larger mass for the models. There are two main reasons for the differences for single crystals. First, the measured mass-diameter relationship and the thickness-diameter ratio

for ice crystals are from different studies, which can produce a selection bias. Second, the thickness-diameter ratio may not be constant over the whole crystal, as we have assumed in our 2-D dendritic shape model. Natural dendrites accumulate more ice to the center of the branches as they grow, which produces less overall mass than our model.

For the aggregate masses (Fig. 3), the agreement between the measurements and shape models is also reasonable, although the modeled aggregates of needles and ordinary dendrites seem to have a factor of about 0.5 less mass than the measurements on average. However, it should be noted that some of the measurements include various mixtures of ice crystal types and their aggregates including both partly melted and rimed snow making a direct comparison unreliable.

A volume observed by a radar is composed of many dissimilar particles in different orientations and sizes. To simulate this, we generate 1000 individual ice crystals for each type randomly chosen within the appropriate size range, and 100 random aggregates of ice crystals for each type and for each number of crystals in the aggregate. For the lump graupels, we use 400 random fractals making the total number of different snowflakes used in this study 8700.

The radar observables are computed by numerically averaging over different size ranges depending on the snowflake type. Also, due to the preferential orientation of the ice crystals, the elevation angle of the radar is varied: 0, 15, 30, 45, 60, 75, and 90 degrees. We assume exponential particle size distribution. In Table 1, we show the size ranges of the various ice crystals and aggregates, and the median volume diameter D_0 values for each snowflake type. The values have been chosen to reflect the natural variation in snowflakes following Pruppacher and Klett (1997).

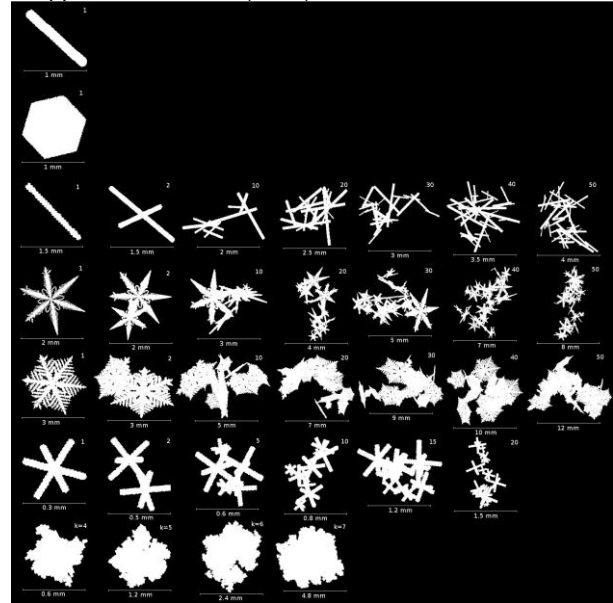


Figure 1: Example shapes of the modeled snowflakes.

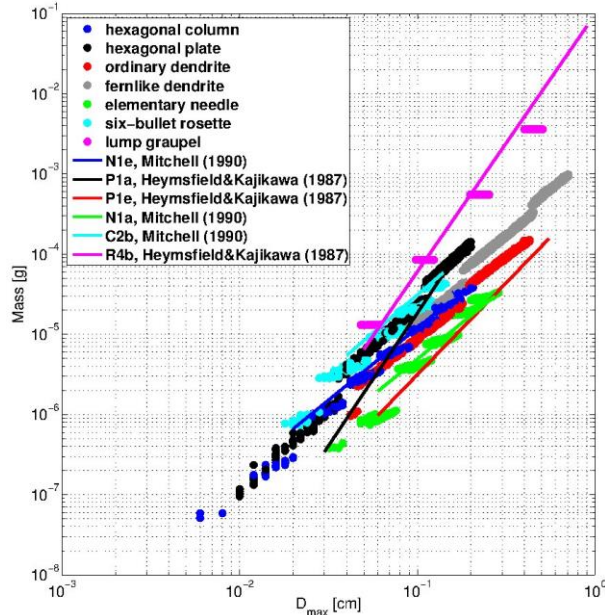


Figure 2: Mass of the modeled single ice crystals as a function of the maximum diameter and corresponding m-D relationships from field measurements.

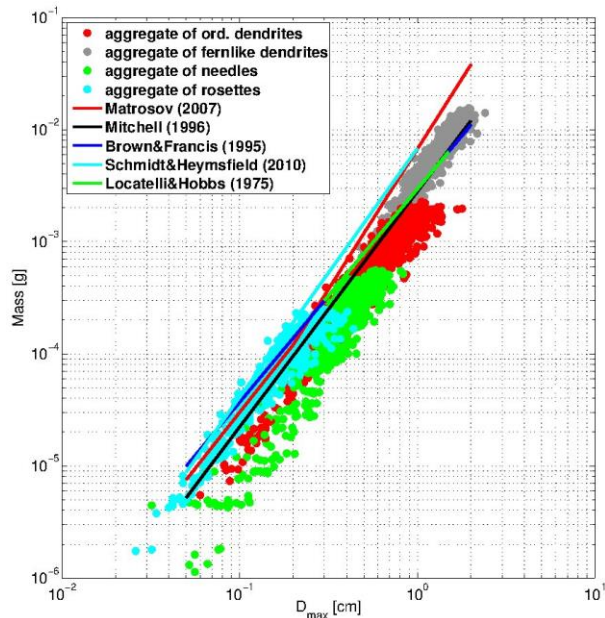


Figure 3: Same as in Fig. 2, but for aggregates.

3. STATISTICAL MEASURES TO ANALYZE A SCATTERING DATASET

Taking into account the various snowflake types used in this study, their PSD parameters, and measurement parameters, such as the elevation angle, radar frequency and radar observables, the resulting data space becomes infeasible to analyze with simple methods. A systematic study of all possible data element combinations is difficult to present in a coherent fashion and does not reveal hidden trends and statistical

significance. However, a large scattering database can be seen as a distribution in a multi-dimensional space and can be analyzed statistically by measuring how well clustered it is with respect to different combinations of measurement parameters. This can help in devising an optimal measurement strategy to characterize falling snow.

The goal in clustering algorithms is to use statistical measures to find a set of clusters from the data set without *a priori* knowledge of the optimal clustering. In our case, the partitions are already known beforehand, so we only need to measure how clustered the partitions are. Although the measures for quantifying data clustering vary, they are commonly called cluster validation indices (CVI). Each CVI is defined in a different way and can have values ranging widely with some having a closed interval of values and some having values up to infinity. Comparing CVI values from different methods can therefore be ambiguous. However, using several methods at the same time can reveal common trends and provide a more reliable basis for determining which combinations of measurement parameters are better than others in characterizing snow. In this study, we have chosen three common internal CVIs: the Davies-Bouldin index (DBI), Dunn index (DI), and the Silhouette index (SI).

4. RESULTS FROM THE STATISTICAL ANALYSIS

Table 2 shows some of the results of analyzing all of the backscattering properties using the statistical measures described in Section 3. Both the optimal frequency bands and elevation angles are shown for each type of measurement. The actual CVI values are not shown. The horizontal reflectivity Z_H by itself is not as good as the other polarimetric observables for characterization, but higher frequencies seem to work better. Ka band shows overall best characterization for both Z_{DR} and the circular depolarization ratio (CDR), while the linear depolarization ratio (LDR) favors even higher frequencies. Middle elevation angles provide best results for Z_{DR} due to smaller variance at higher angles, while CDR favors low angles. However, there is no common trends for the other observables.

For the dual-frequency ratios (DFRs), higher frequencies provide better characterization. However, slightly off-nadir measurements seem to be better than nadir measurements. This may be due to the fact that at slightly off-nadir direction, the oriented ice crystals appear more asymmetrical and therefore more non-spherical, which increases the variation in the backscattering cross sections. Having a large difference in frequencies results in worse characterization than having two higher frequencies. When combining two DFRs, which share one frequency, higher frequencies are better. Ka band is optimal, when combining DFR and Z_{DR} . There does not seem to be any noticeable trend with the optimal elevation angles for DFR combinations.

Measurement	Optimal freq. band			Optimal elev. Angle [deg]		
	DBI	DI	SI	DBI	DI	SI
ZH	S	W	W	45	75	0
ZDR	Ka	Ka	W	60	60	60
LDR	W	W	Ka	60	0	90
CDR	W	Ka	Ka	0	0	0
DFR Ku/Ka	-	-	-	30	30	75
DFR Ka/W	-	-	-	75	15	0
DFR W/220	-	-	-	90	30	75
DFR Ku/Ka + Z _{DR,Ku}	-	-	-	0	30	0
DFR Ku/Ka + DFR Ka/W	-	-	-	45	30	90
DFR Ka/w + DFR W/220	-	-	-	90	15	75
ZDR + CDR	Ka	Ka	W	75	60	0

Table 2: Cluster validation for the backscattering properties using the Davies-Bouldin (DBI), Dunn (DI), and the Silhouette (SI) indices. Bold font marks the overall best clustering for each index.

5. EXAMPLE COMBINATIONS OF MEASUREMENTS

Fig. 4 shows the $DFR_{Ku/Ka}$ and $DFR_{Ka/W}$ combination plotted together at 90 deg elevation angle. The results are similar to those in studies by Kneifel et al. (2011) and Leinonen et al. (2012) showing that the aggregates separate from the more spherical graupels, which have larger $DFR_{Ka/W}$ values. This indicates that higher-frequency measurements near nadir that produce DFRs similar to spheroidal models may be due to heavily rimed snow or graupel. Note that single crystals are impossible to characterize at 90 deg elevation due to the preferential orientation of the crystals, which produces Rayleigh-type backscattering. However, at lower elevation angles they show larger separation with the dendrites and hexagonal plates clearly separating from the aggregates. On the other hand, different aggregate types are also difficult to distinguish from each other.

In Fig. 5, we show ZDR and CDR plotted together at the Ka band and at 0 deg elevation angle. As can be seen, this provides a fairly good characterization and produces five different clusters/snow types: hexagonal plates, dendrites, columns/needles, aggregates, and graupels/rosettes. It should be noted that measurement limits and attenuation of the radar signal have not been taken into account, when computing the CVIs, which may result in unpractical characterization in some cases.

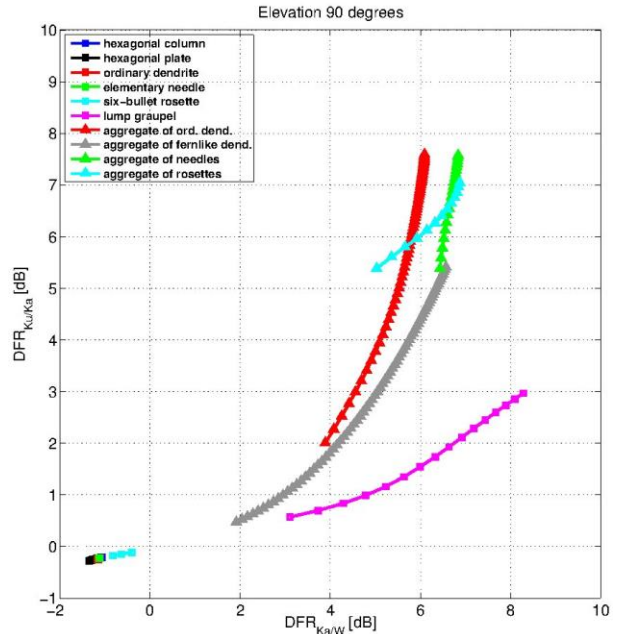


Figure 4: Dual-frequency ratios $DFR_{Ku/Ka}$ and $DFR_{Ka/W}$ at 90 deg elevation angle for the models.

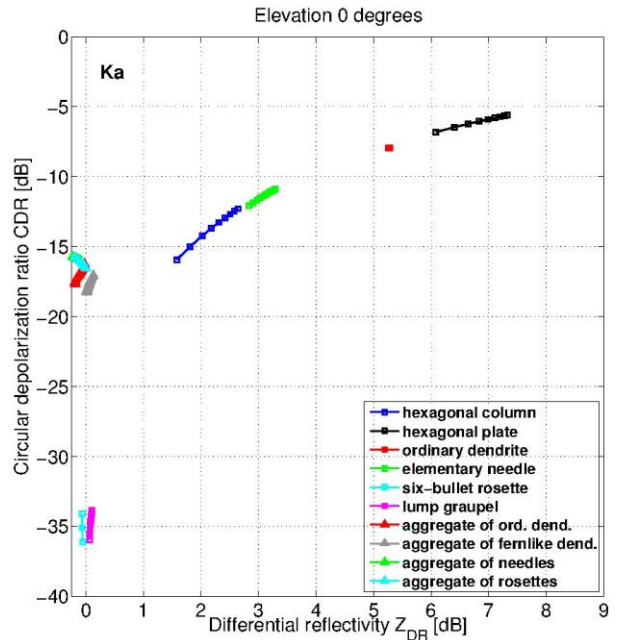


Figure 5: CDR and Z_{DR} for the modeled snowflakes at the Ka band and at 0 deg elevation angle.

6. SNOWFALL CASE DURING GCPEX

The goal of the GPM Cold-season Precipitation Experiment (GCPEX) was to study how passive and active multi-frequency sensors could characterize falling snow by collecting both in situ microphysical and remote sensing data. In this study, we use the measurement data from the mobile NASA D3R ground-based radar, which is a dual-polarization Doppler radar operating at Ku and Ka bands, and the APR2 radar onboard the

NASA DC-8 aircraft also operating at Ku and Ka bands. For this case study, we have selected 27th of January at 03:05 AM during which snow was reported falling.

D3R radar was operating close to the DC-8 aircraft route and scanning within 15 deg in the azimuthal direction from the aircraft flight path (see Fig. 6). The APR2 radar was pointing towards the ground. We do not use the Ka data from D3R due to attenuation problems.

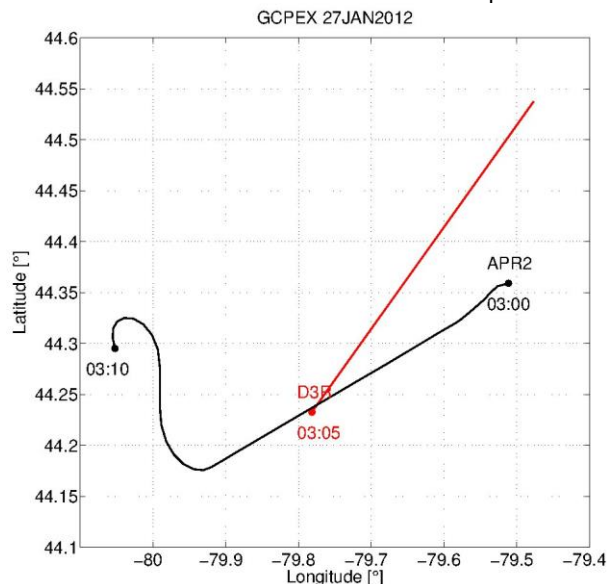


Figure 6: Location and measurement direction of D3R radar (red) and the flight path of APR2 radar (black).

In Fig. 7, we show Z_H and Z_{DR} measured by D3R, and the $DFR_{Ku/Ka}$ measured by APR2 matched in range and height. There is a melting layer above 1 km altitude with a visible bright band. Between 2 and 4 km altitudes, there are two bright areas driven by wind shear. These areas are associated with low Z_{DR} values (< 1 dB) indicating aggregates. There are also many areas close to the aggregation which show larger Z_{DR} values and lower Z_H values indicating possible ice crystals. To verify this, we plot Z_{DR} (D3R) and $DFR_{Ku/Ka}$ (APR2) together with all matching range-height cells above 2 km altitude in Fig. 8. Results from the DDA computations are also shown for both needles (green symbols) and ordinary dendrites (red symbols). For the computations, we have mixed the single ice crystals and aggregates together by varying the mixing ratios, and D_0 for both crystals and aggregates. As can be seen, dendrites and aggregates of dendrites seem to be the more likely candidates due to the larger span of values coinciding with the radar measurements. Also, for Z_{DR} there seems to be an average signal of about 0.5 dB for aggregates (large DFR values), which indicates that the assumption of random orientation may not be appropriate here. This value is the same as shown by Hogan et al. (2012).

Note that due to the temporal and spatial differences of D3R and APR2 in this case, a good volume matching is impossible to do. This may explain the large variance of values. Also, adding airborne

microphysical probe data to the analysis may further narrow down the possible model parameters.

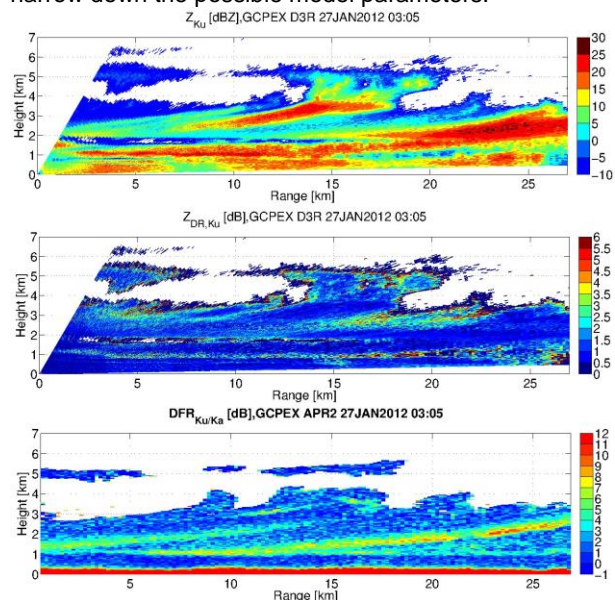


Figure 7: Horizontal reflectivity (top panel) and differential reflectivity (middle panel) measured by D3R, and dual-frequency ratio at Ku and Ka bands measured by APR2 radar (bottom panel). The measurements were taken during the GCPEX campaign in January 27th, 2012.

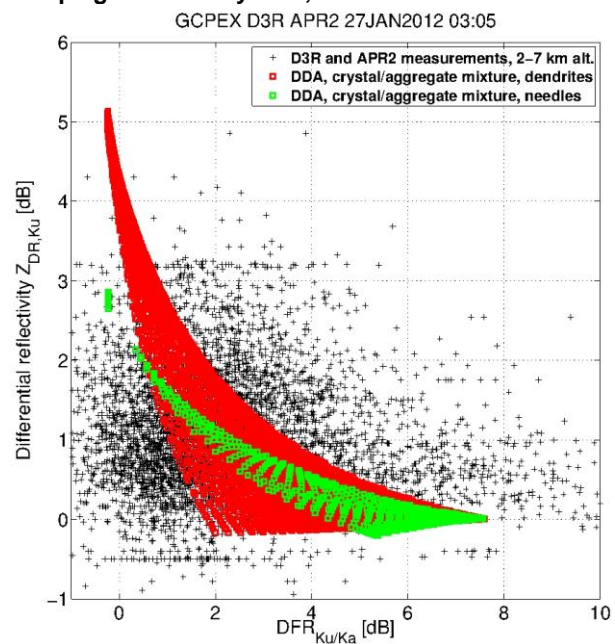


Figure 8: The differential reflectivity from D3R and $DFR_{Ku/Ka}$ from APR2 plotted with DDA computations for needles (green symbols) and dendrites (red symbols).

7. CONCLUSIONS

In the present study, we have modeled physically realistic snowflakes of various shapes and sizes to analyze their size-integrated backscattering properties. The backscattering properties have been computed at C, S, X, Ku, Ka, W, and 220 GHz bands and then compared to radar observations in order to characterize snowflake types.

The results confirm that DFRs, especially at higher radar frequencies, are promising measurements to characterize snow, as already demonstrated by other studies (Kneifel 2011; Leinonen 2012). They also show that, in principle, using even higher frequency bands (220 GHz) than W can improve the characterization. However, attenuation of the radar signal can become problematic at such high frequency range, and may hinder its applicability. The transition region from Rayleigh scattering to the resonance region between Ku and Ka bands seems to provide overall the best characterization, while also avoiding the possible attenuation problems.

The presence of single, preferentially oriented ice crystals has a profound effect on the polarimetric backscattering properties. The results indicate that Z_{DR} and the depolarization ratios (LDR, CDR) provide better characterization than DFRs and this is enhanced even further by combining these measurements together.

When the computations are compared to radar measurements from aircraft and ground, the results show that modeling together with dual-polarization multi-frequency measurements can be used to characterize snow. They also demonstrate the advantage of combining dual-polarization measurements, especially Z_{DR} , with DFRs, which can narrow down characterization. Additional advantage of using these observables is that they are both independent on the intercept parameters in PSDs and therefore require less assumptions of the snowfall.

8. ACKNOWLEDGMENTS

We want to thank the Finnish IT Center for Science (CSC) for providing the computational resources to do the study. This work was supported by the Finnish Cultural Foundation and the NASA PMM program.

REFERENCES

- Cho, H. R., J. V. Iribarne, and W. G. Richards, 1981: On the orientation of ice crystals in a cumulonimbus cloud. *J. Atmos. Sci.*, **38**, 1111-1114.
- Hogan, R. J., L. Tian, P. R. A. Brown, C. D. Westbrook, A. J. Heymsfield, and J. D. Eastment, 2012: Radar scattering from ice aggregates using the horizontally aligned oblate spheroid approximation. *J. Appl. Meteor. Clim.*, **51**, 655-671.
- Ishimoto, H., 2008: Radar backscattering computations for fractal-shaped snowflakes. *J. Meteor. Soc. Japan*, **86**, 459-469.

Kneifel, S., M. Kulie, and R. Bennartz, 2011: A triple frequency approach to retrieve microphysical snowfall parameters. *J. Geophys. Res.*, **116**, D11203.

Leinonen, J., S. Kneifel, D. Moisseev, J. Tyynelä, S. Tanelli, T. Nousiainen, 2012: Evidence of nonspheroidal behavior in millimeter-wavelength radar observations of snowfall. *J. Geophys. Res.*, **117**, D18205.

Noel, V., and K. Sassen, 2005: Study of planar ice crystal orientations in ice clouds from scanning polarization lidar observations. *J. Appl. Meteor.*, **44**, 653-664.

Petty, G. W., and W. Huang, 2010: Microwave backscatter and extinction by soft ice spheres and complex snow aggregates. *J. Atmos. Sci.*, **67**, 769-787.

Pruppacher, H. R., and J. D. Klett, 1997: Microphysics of clouds and precipitation. Dordrecht, Boston.

Tyynelä, J., J. Leinonen, D. Moisseev, and T. Nousiainen, 2011: Radar backscattering from snowflakes: comparison of fractal, aggregate and soft-spheroid models. *J. Atmos. Oceanic Technol.*, **28**, 1365-1372.

Westbrook, C. D., 2004: Universality in snow formation, PhD thesis, University of Warwick, Coventry, UK.

Westbrook, C. D., R. C. Ball, P. R. Field, 2006: Radar scattering by aggregate snowflakes. *Q. J. R. Meteorol. Soc.*, **128**, 1-17.